Multiphysics Simulation of an Electrostatics-Rotary MEMS Stepper Motor

G.S. Abarca-Jiménez¹, L. Sánchez-Márquez², J. Mares-Carreño^{1*}, M. A. Reyes-Barranca², L.G. Corona-Ramírez³

¹Unidad Profesional Interdisciplinaria de Ingeniería Campus Hidalgo, UPIIH IPN Hidalgo, México Carretera Pachuca-Actopan km 1+500, San Agustín Tlaxiaca, 42162

²Electrical Engineering Department, CINVESTAV IPN Mexico City, Mexico Av. Instituto Politécnico Nacional 2508, Gustavo A. Madero, San Pedro Zacatenco, 07360

³Unidad Profesional Interdisciplinaria de Ingeniería y Tecnologías Avanzadas, UPIITA IPN, Mexico City, Mexico Av. Instituto Politécnico Nacional 2580, La Laguna Ticomán, Gustavo A. Madero, 07340

Abstract

This paper shows the multiphysics simulation process of a rotary MEMS stepper motor with electrostatic actuation, where the solid mechanics, electrostatics, and moving mesh simulations through COMSOL are considered in a time-dependent study. The rotary MEMS motor comprises the aluminum structural layer from a 0.5µm CMOS technology used for integrated circuit fabrication. Both the rotor and the stator are immersed in a dielectric; for this reason, the simulation requires a moving mesh to model the electrical characteristics of the medium. A mesh convergence study is conducted to ensure the accuracy and mesh independence of the results. The simulation also considers the frequency of the stator electrodes alternating signal and the frequency response of the rotor to define the solver time stepping. Through this simulation, it was possible to verify that the micrometric electrostatic actuator has an angular displacement with a linear trend, which allows the proposed design to be verified.

Keywords: Multiphysics simulation, MEMS stepper motor, electrostatic actuation, time dependent simulation, mesh convergence, moving mesh.

1. Introduction

Finite Element Analysis (FEA) is a powerful and handy tool in engineering design that has become a crucial part of the design process of many products in a broad range of applications. The FEA has become a constant in the design of microelectromechanical systems (MEMS) [1] [2] [3] [4] [5], as it allows the designer to consider all the involved physics in the operation of MEMS sensors and actuators in only one model, obtaining complete information for decision-making [6] [7] [8].

Multiphysics is inherent to MEMS actuators, as the typical mechanisms of actuation are thermal, piezoelectric, electrostatic, or magnetic, all deriving from a desired structural mechanics behavior. The simulation of a MEMS actuator must then consider all the physics involved in the operation and the couplings between them in a suitable way.

When it comes to a rotary stepper motor, the significance of studying its time-dependent behavior cannot be overstated. Time-dependent FEA plays a crucial role in this, considering the frequency response of the system, the time-dependent boundary conditions and nonlinearities, to define the proper solver parameters [9][10][11]. Another key consideration during the time-dependent simulation of the rotary stepper motor is the deformation or movement of the surrounding medium, which is particularly relevant for the electrostatic actuation as the surrounding medium serves as the dielectric needed for the electrostatic actuation to occur.

2. Rotary MEMS Stepper Motor Design

Micromotors are actuators that generate movement due to some micro-activation force and can be fabricated based on MEMS-dedicated technologies, like POLYMUMPS or METALMUMPS. Actuation forces for micromotors are primarily electrostatic, generated by misaligned and electrically energized plates, which generate electrostatic forces, thus stimulating the motor movement.

This work focuses on an electrostatically actuated rotary MEMS stepping motor (Figure 1 and 2), made up of a one-piece rotor with multiple teeth (A, A') and a stator comprised of multiple fixed electrodes (S1, S2, S3). The rotor and stator are formed of conductive material, particularly aluminum, as the micromotor's structural layer.

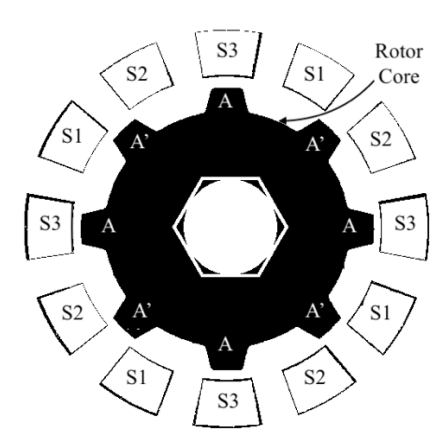


Figure 1. The top view of an angular micromotor, the rotor, and the stator comprised of a conductive material.

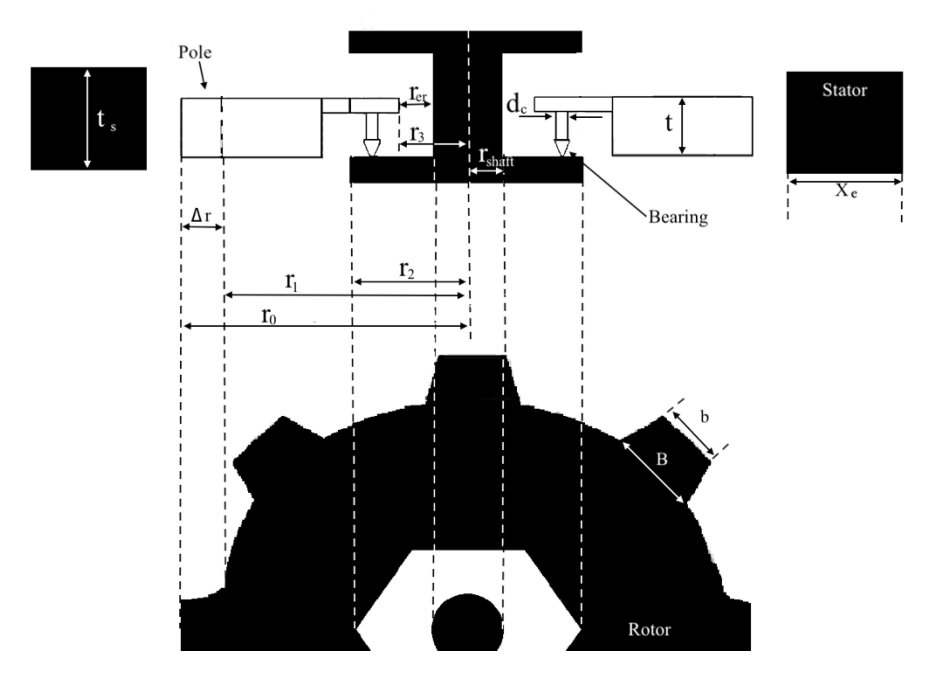


Figure 2. Morphological parameters of the micromotor.

The morphological parameters listed in Table 1 optimally relate electromechanical performance and On-Semi manufacturing rules.

Table 1. Morphological parameters of the micromotor. Geometrical parameters are illustrated in Fig. 2; Ns is the number of poles in the stator and Nr is the number of poles in the rotor.

Morphological paran	neter Metrics Mor	phological paran	neter Metrics
t	2.31µm	$t_{\scriptscriptstyle \mathcal{S}}$	5.277μm
r_1	200μm	r_0	218µm
r_2	180μm	r_3	53 μm
N_{s}	75	N_r	50
Δr	18μm	r_{shaft}	50μm
В	15μm	r_{er}	3µm
b	9µm	r_c	57.2μm
r_T	241.6µm	r_{shield}	57.2μm
x_e	20μm	t_o	0.57µm
d	3.6µm	d_c	1.2µm

During operation of the MEMS stepper motor, two main forces are considered, the friction force that must be overcome for the motor to rotate, given by equation 1, and the electrostatic force which actuates the motor, given by equation 2.

$$F_f = \mu \rho g V \tag{1}$$

Where:

 $\mu \rightarrow Static\ friction\ coefficient$

$$\rho \to Density \left[\frac{kg}{m^3} \right]$$

 $g \to Gravitational\ acceleration\ \left[\frac{m}{s^2}\right]$

 $V \rightarrow Volume \ of \ the \ rotor[m^3]$

$$F_e = N_s \varepsilon_r \varepsilon_o \frac{t}{2d} V_o^2 \tag{2}$$

Where:

 $N_s \rightarrow Number\ of\ active\ stator\ poles$

 $\varepsilon_r \to Relative\ permittivity\ of\ the\ medium$

 $\varepsilon_0 \to Relative\ permittivity\ of\ vaccum[^F/_m]$

 $V_o \rightarrow Driving\ voltage\ [V]$

The stator has 75 poles, activated only in groups of 50 at a time, to establish a specific 'geometric relationship' between the rotor and stator poles. This relationship, which is 2/3, as shown in [12] and [13], is a fundamental aspect of the motor design. The electrostatic force must be greater than the friction force for the motor to move. In this case, the coefficient of static friction to consider is the one present between the upper aluminum layer and the lower aluminum layer, which is the area where the rotor bearings and the rotor base come into contact (see Fig. 2). However, the value of the coefficient of static friction to be considered is uncertain as the possible drop effect, the roughness of the surface after the machining and the scarce experimental data are too challenging to be accurately measured, so to take the friction force into account it is suggested to give the static friction coefficient a value between 1 and 3, as is done in [14][15].

Given the above, the necessary voltage to drive the MEMS stepper motor can be computed from equation 2 by assuming that the electrostatic force equals the friction force. Then, the minimum driving voltage for static friction coefficients between 1 and 3 is:

$$\mu = 1, V_o > 4.98 V$$

$$\mu = 2, V_o > 7.04 V$$
(3)

$$\mu = 3, V_o > 8.63 V$$

This voltage range can be considered low and feasible for the application analyzed here.

3. Methods: The Finite Element Model

Finite element analyses were performed to validate the design of the MEMS stepper motor. Remember that this stepper motor is actuated with electrostatic forces, so it is necessary to consider the variables involved in the physical phenomenon, such as a moving mesh for the dielectric fluid involved and the displacement that the electrostatic force will cause on the motor. Therefore, this analysis is multiphysics in nature.

The FEM model of the motor has the following considerations:

• The CAD model of the MEMS stepper motor (Figure 3), comprising the 50-tooth rotor, 75 stator poles, bearings, and a bearing base, was drawn based on the morphological parameters in Table 1. In addition, a block was designed to represent the dielectric that surrounds the motor, the stator, and the bearings.

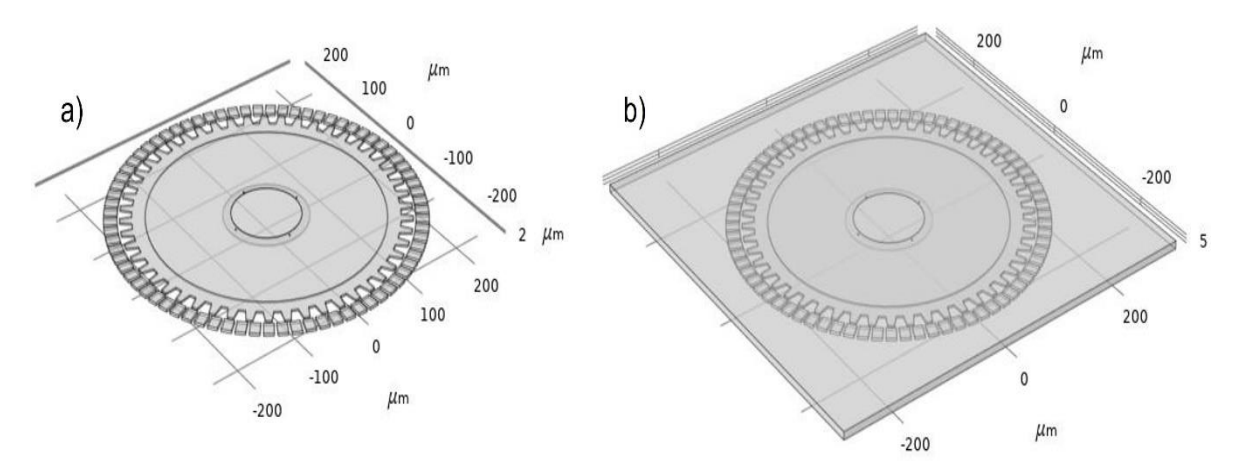


Figure 3. 3D CAD model of the MEMS stepper motor a) without surrounding block b) With surrounding block.

- Determination of the desired physics to solve for in the analysis. Electrostatic forces impulse the stepping motor; two physics are involved: electrostatics and solid mechanics, coupled by an electrostatic force interface.
- Determination of the analysis space dimension. Even though the motor's movement is limited to a single plane, the spatial dimension of the analysis will be 3D as simplifying due to the motor's topology is not possible.
- Selection of the type of study. Given that the 75 stator electrodes are activated in groups of 25 to cause
 the motor's rotation, the type of study will be time-dependent on being able to capture the stator
 electrodes' commutation and the effect of said commutation on the rotor's rotary displacement.
- Simulation time. The stator electrodes are turned on and off sequentially to obtain the desired motion of the rotor; for this design, an operation frequency of 500 Hz is established. This means that every 2ms, all three groups of the stator electrodes commute from on to off once, as shown in Figure 4. Two cycles of 2ms were simulated to show stable and repetitive behavior.

Density

ISSN: 1750-9548

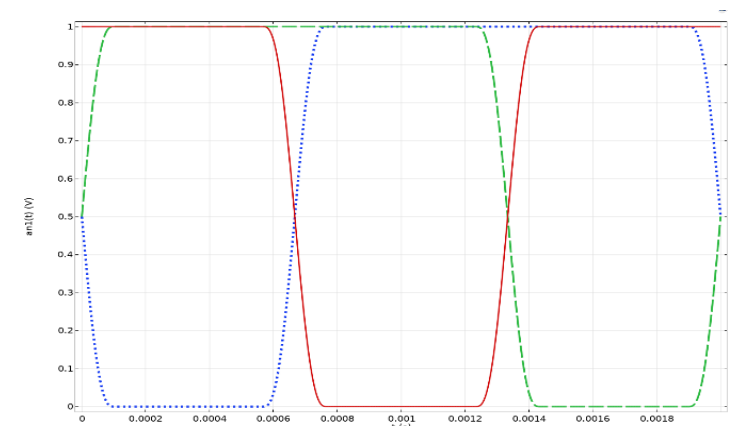


Figure 4. Stator electrodes signals.

Material property data. As mentioned in the previous section, the rotor, stator, and bearings are all
made of conductive materials, in this case, aluminum. The block surrounding the rotor, stator, and
bearings has air properties. The properties of both materials are in Table 2.

Aluminum		Air		
Property	Value	Property	Value	
Young modulus	70e9 Pa	Relative permittivity	1	
Poisson's ratio	0.33			

 $2700 \ kg/m^3$

Table 2. Assumed values for material properties.

- Definition of boundary conditions. The boundary conditions for the solid mechanics interface are fixed constraints over all the stator electrodes and a rigid connector for the internal cylindrical face of the rotor, which only allows rotation around the z-axis. On the other hand, for the electrostatic interface, the boundary conditions are four voltages, one for the rotor and one for each of the three groups of 25 electrodes of the stator; these three voltages are variable in time (Figure 4).
- Mesh generation. A tetrahedral mesh is used for meshing all the domains; a local mesh control over the tip of the rotor teeth and the front of the electrodes is added to control the number of elements in these entities since the area between them is responsible for the movement of the rotor via electrostatics. A mesh of the whole model is shown in Figure 5a, and the mesh for the rotor and stator is shown in Figure 5b.

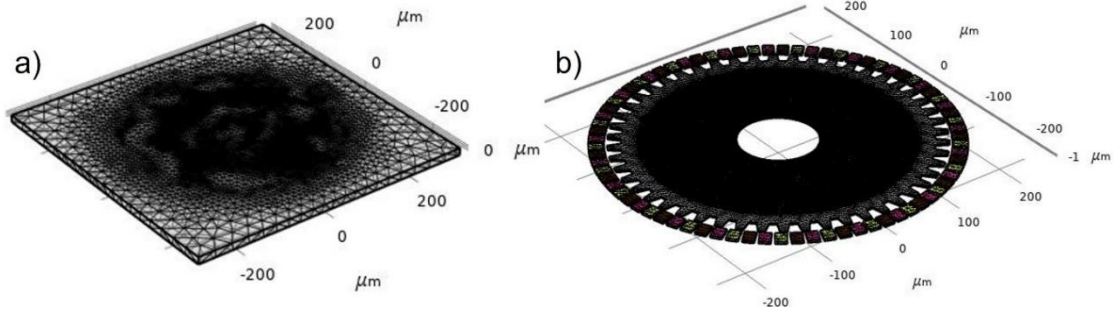


Figure 5. a) Mesh of the entire model b) Mesh of the rotor and stator.

In any analysis, the mesh element size is essential since the problem's solution is calculated at discrete points (nodes) of the elements. The elementary and global results are generated based on these point solutions by applying techniques like interpolation or quadrature. So, to get accurate results, more nodes are required, which can be achieved by using smaller or higher degree elements. However, adding more nodes does not guarantee more accurate results by itself. To demonstrate the accuracy of the results the mesh size must be independent of the convergence. [16] [17] [18] [19].

To assure the accuracy of the results from the multiphysics analysis of the rotary MEMS stepper motor, a mesh convergence study was developed by doing a series of subsequent analyses refining the mesh at the tip of the rotor teeth and the corresponding faces of the stator electrodes (Figure 6). This refinement region is between the rotor teeth and stator electrodes, where the electrostatic forces that move the motor are generated [14].

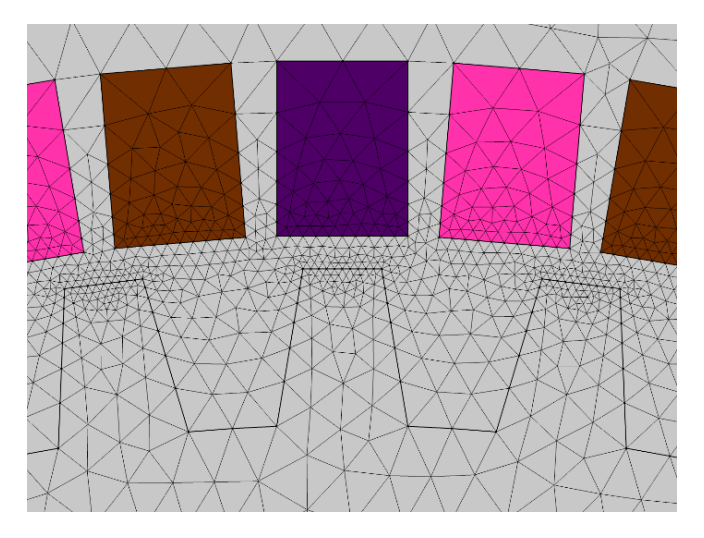


Figure 6. Mesh local control at teeth tip.

A graph of the displacement of the tooth tip against the number of elements at the tip of a rotor tooth was made (Figure 7). The results plotted correspond to the total displacement of a specific tooth tip at 1 ms of simulation time. The graph shows that mesh convergence is achieved with ten mesh elements at the tip of the rotor teeth.

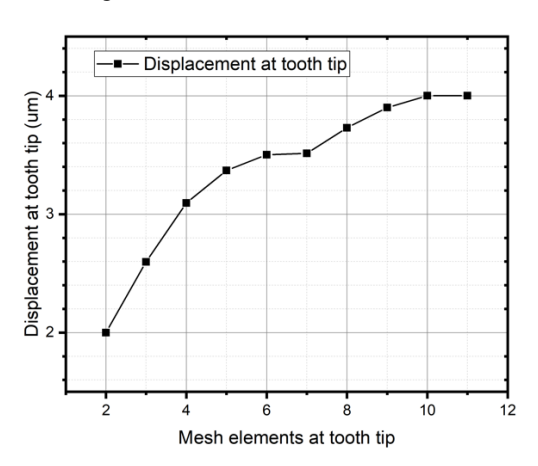


Figure 7. Mesh convergence graph.

Hence, this mesh density was used after these results since accuracy was achieved with the multiphysics analyses.

When a multiphysics analysis is made, it's essential to consider how the different physics will relate and how to obtain solutions for all the involved unknowns. For the rotary MEMS stepper motor analysis, the solid

Volume 18, No. 2, 2024

ISSN: 1750-9548

mechanics and electrostatics physics are related by the electrostatic force, which is the driving force of the rotor and is calculated from the Maxwell stress tensor employing integration of equation 4 over the surfaces on which the force acts [20]. Maxwell's stress tensor exists for all dielectric materials, including air.

$$\vec{n}F_{e} = \frac{1}{2}\vec{n}(\vec{E}\cdot\vec{D}) + (\vec{n}\cdot\vec{E})\vec{D}^{T}$$

$$where:$$

$$\vec{E} \rightarrow Electric\ field\ \begin{bmatrix} V/_{m^{2}} \end{bmatrix}$$

$$\vec{D} \rightarrow Electric\ displacement\ \begin{bmatrix} C/_{m^{2}} \end{bmatrix}$$

$$\vec{n} \rightarrow Outwards\ normal\ vector$$

$$(4)$$

As seen in equation 4, to calculate the electrostatic force, it is necessary to first know the electric field and the electric displacement. Once the electrostatic force is known, the solid mechanics can be solved. Thus, the solution of the physics involved must be segregated, which means solving the electrostatics first, followed by the solid mechanics.

Another consideration for the rotary motor simulation is the dielectric medium (air) movement, whose mesh must be dynamic since the domain that defines the dielectric medium will change its shape due to the movement of the rotor, adding new unknowns to be calculated in the simulation in the form of a spatial displacement field of the moving mesh [21][22]. Next, the segregated solution for the spatial mesh displacement is calculated after properly determining the displacement field associated with the solid mechanics.

On the other hand, the voltages applied to the three groups of stator electrodes are defined by a step function, which implies an instantaneous change in time. Boundary conditions with instantaneous changes must be treated with care, as a deficient treatment of these can lead to an extremely small time-step to compute the solution, which in turn causes very long solution times or even convergence issues. For the case presented here, the strategy used for the treatment of stator electrode voltages is to stop the solver once the switching times of the signals are reached and then reinitialize the solver based on the previous results and the updated boundary conditions.

Like the voltage switching time, the spatial displacement and distortion of the moving mesh are monitored at every time step since excessive distortion will lead to ill results or convergence issues. A maximum distortion of 3.5 is considered a reliable criterion, and when this value is exceeded, the solver stops, and a re-meshing over the deformed geometry is carried out.

Finally, a time step for the time-dependent solver is defined considering the switching frequency of the voltages and the frequency response of the rotor, resulting in a time step of 1x10-5 seconds.

4. Results

The results obtained include the magnitude and angle of the displacement vector over the X-Y plane at the tip of one tooth of the rotor. As seen in Figure 8, the magnitude of the vector displacement in the X-Y plane of the micromotor surpasses $100 \mu m$ in 0.003 s, while the angle of the vector displacement reaches 193.5 degrees when 18 V is applied. Figure 8 shows that the response of the micromotor is nonlinear from 0ms to 1 ms since the simulation starts from an initial state of rest. Then, this period's response is the micromotor's transient response.

Conversely, for times from 1ms to 3ms, the micro motor displays a linear response (Figure 8), which is regarded as the steady state of the response. Over the steady part of the response, a curve fit was made (Figure 9), from which two linear functions (Equation 5) and (Equation 6) were obtained. The linear behavior of both graphs is indicative that the magnitude and angle of the displacement vector at the tip of one teeth of the rotor are varying at a constant rate given by the slopes of the linear functions (Equation 5) and (Equation 6) respectively. This, in turn, implies a constant angular velocity for the rotor, a crucial factor in the micromotor's performance and design.

$$D = 44.4534t - 30.9734 \tag{5}$$

$$A = 5.9t + 175.576 \tag{6}$$

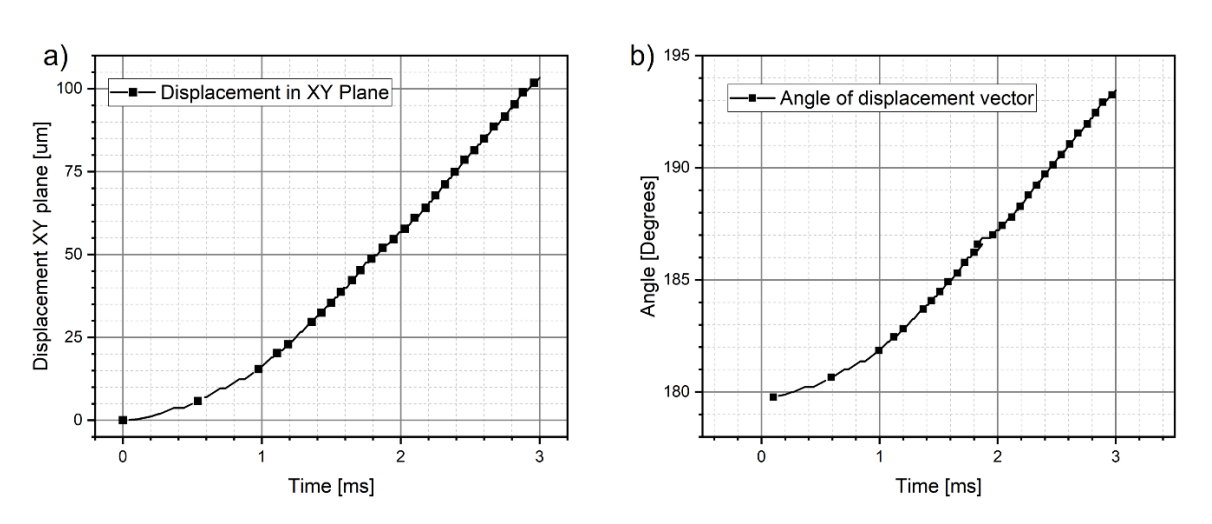


Figure 8. Mesh convergence graph Graphs of rotor displacement with a positive 18V voltage applied. a) Displacement vector magnitude in X-Y plane b) Angle of displacement vector in X-Y plane.

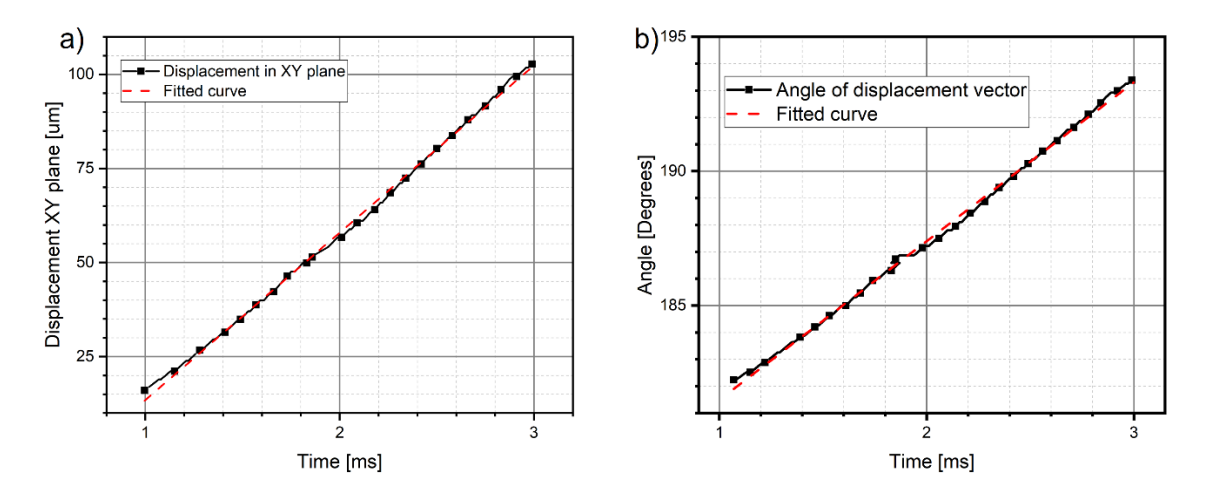


Figure 9. Curve fit over the steady part of the response of the micromotor a) Displacement vector magnitude in X-Y plane b) Angle of displacement vector in X-Y plane.

Equation 5 can compute the expected magnitude of the displacement vector in the X-Y plane for the rotor at any given time, and equation 6 can also compute the angle of the displacement vector at any time.

Figure 10 a) shows the electric potential along with the displacement vector of the rotor in the X-Y plane, while Figure 10 b) shows the electric field norm between the rotor and stator along with the displacement vector in the X-Y plane; both images were taken for t=0.00129 ms. A comparison of both images in Figure 10 shows the match between the stator electrode at 0V and the produced electric field, which is maximum at the front border

of the stator electrode, producing the necessary electrostatic force to move the rotor. Finally, with the proposed simulation strategy, there were no convergence problems, and the full simulation of the 3 ms took 101 hours and 2 minutes to complete.

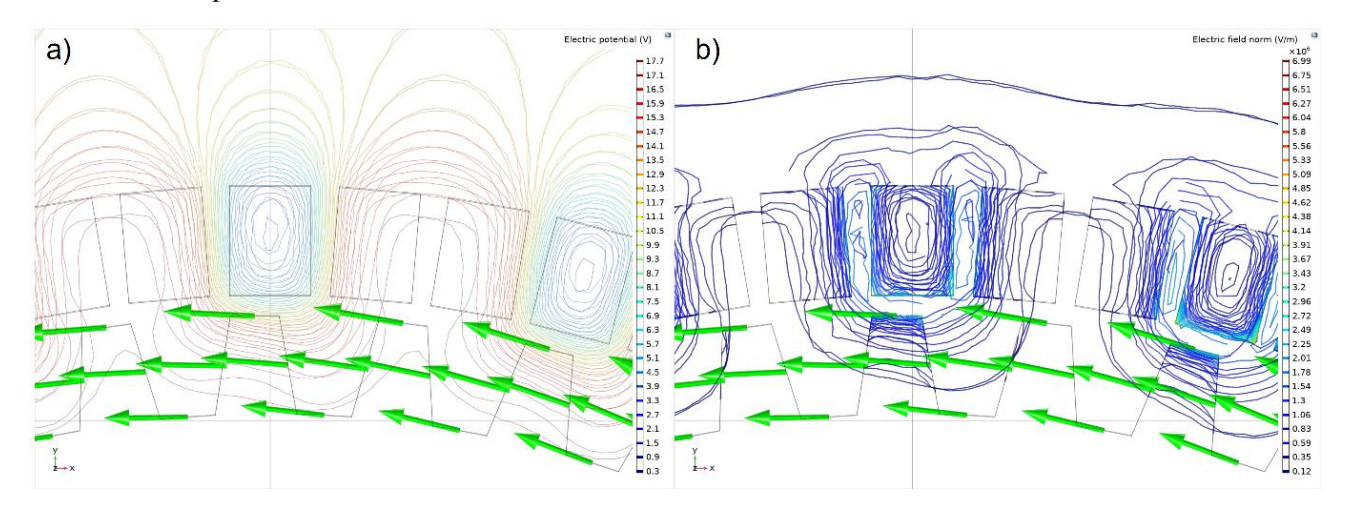


Figure 10. Results at time t=1.29 ms a) Electric potential and displacement vector in X-Y plane b) Electric field norm and displacement vector in X-Y plane.

5. Discussion

The operation of the rotary micromotor could be validated by performing a multiphysics simulation that considers the electrostatic actuation mechanism step by step and the time dependence of the stator electrode signals. The behavior of the rotary movement of the micromotor tends to be linear in accordance with what was designed.

The multiphysics simulation is a fundamental tool in the MEMS design and development process since it allows the study of the operation of the proposed designs, considering all the conditions and physical phenomena involved in the operation of the MEMS sensors and actuators. This provides complete information to the development team for better decision-making prior to the manufacturing process.

During the simulation process, good preparation of the mesh, a mesh convergence study, and the correct application of boundary conditions that emulate the operating conditions allowed accurate results. For time-dependent simulations, the correct definition of the solver time stepping allows to avoid convergence problems and helps to shorten solution times.

Acknowledgments

The work in this paper is in part supported by Secretaría de Investigación y Posgrado del Instituto Politécnico Nacional, and the Unidad Profesional Interdisciplinaria de Ingeniería Campus Hidalgo- Instituto Politécnico Nacional (Grant No. 20241962 and 20241688).

References

- [1] Chyuan S., Computational simulation for MEMS combdrive levitation using FEM, Journal of Electrostatics, (2008), Vol. 66, pp. 361-365, https://doi.org/10.1016/j.elstat.2008.03.005
- [2] Roy, A.; Nabi, M., Modeling of MEMS Electrothermal Microgripper employing POD-DEIM and POD method, Microelectronics Reliability, (2021) Vol. 125, https://doi.org/10.1016/j.microrel.2021.114338.
- [3] Sharma, K., Karmakar, A., Prakash, K., Design and characterization of RF MEMS capacitive shunt switch for X, Ku, K and Ka band applications, Microelectronic Engineering, (2020) Vol. 227, https://doi.org/10.1016/j.mee.2020.111310.

- [4] Abarca Jiménez G.S., Mares Carreño J., Mendoza Acevedo S., Reyes Barranca M.A, Alemán Arce M.A., Munguía Cervantes J.E, Granados Rojas B., 2019 "Validation of a CMOS-MEMS accelerometer based on FGMOS transduction by electromechanical modification of its coupling coefficient", ISSN: 14321858.
- [5] Abarca Jiménez G.S., Mares Carreño J., Mendoza Acevedo S., Reyes Barranca M.A, Alemán Arce M.A., Munguía Cervantes J.E, Granados Rojas B., 2018 "Inertial sensing MEMS device using a floating gate MOS transistor as transducer by means of modifying the capacitance associated to the FGMOS", ISSN: 14321858.
- [6] Allameh, M.; Shafai, C., Tri-electrode MEMS electrostatic actuator with lower control voltage and higher stroke for actuator array implementations, Journal of electrostatics, (2021) Vol. 114, https://doi.org/10.1016/j.elstat.2021.103635Get
- [7] Kolli, V.R.; Dudla, P.; Talabattula, S., Integrated optical MEMS serially coupled double racetrack resonator based accelerometer, Optik, (2021), Vol. 236, https://doi.org/10.1016/j.ijleo.2021.166583
- [8] Xie, Y.; Wang, Y.; Yi, Z., Qin, M., Huang, Q., Simulation and experiment of miniaturized housing structure for MEMS thermal wind sensors, Sensors and Actuators A: Physical, (2022), Vol. 333, https://doi.org/10.1016/j.sna.2021.113297
- [9] Soderlind, G., Time-step selection algorithms: Adaptivity, control, and signal processing, Applied numerical mathematics, (2006) Vol. 26, https://doi.org/10.1016/j.apnum.2005.04.026.
- [10] Vugdelija, M.; Stijanovic, Z.; Stojanovic, Z., Determination of a time step interval in hydraulic systems transients simulation, Advances in engineering software, (2000) Vol. 31, https://doi.org/10.1016/S0965-9978(99)00043-5
- [11] Xu Li, Xiaokang Li, Yongkang Wu, Lizhou Wu, Zurun Yue, Selection criteria of mesh size and time step in FEM analysis of highly nonlinear unsaturated seepage process, Computers and Geotechnics, (2022) Vol. 146, https://doi.org/10.1016/j.compgeo.2022.104712.
- [12] Basha M. A. and Safavi-Naeinin S. Optimization of electrostatic side-drive micromotor torque using a new rotor-pole-shaping technique, Optomechatronic Actuators, Manipulation, and Systems Control (2006). https://doi.org/10.1117/12.687698
- [13] Ferreira-Vinhais H., Henrique de Godoy O. and Nelli-Silva E. C., Optimized Design of an Electrostatic Side-Drive Micromotor. ABCM Symposium Series in Mechatronics (2006) Vol. 2: 433-450.
- [14] Reddy R. R., Okamoto Y. and Mita Y., An on-chip test structure for studying the frictional behavior of deep-RIE MEMS sidewall surfaces. IEEE International Conference on Microelectronic Test Structures (ICMTS), (2018) pp. 173-178, DOI: 10.1109/ICMTS.2018.8383792.
- [15] Meng G., Zhang Wen-Ming, Huang H., Li Hong-Guang and Chen D., Micro-rotor dynamics for micro-electro-mechanical Systems (MEMS). Chaos, Solutions & Fractals, (2004) Vol. 40: 538-562. https://doi.org/10.1016/j.chaos.2007.08.003
- [16] Patil, H.; Jeyakarthikeyan, P.V.; (2018), Mesh convergence study and estimation of discretization error of hub in clutch disc with integration of ANSYS, IOP Conf. Ser.: Mater. Sci. Eng. (2018) Vol. 402. DOI 10.1088/1757-899X/402/1/012065
- [17] Morris, A.; A practical guide to reliable finite element modelling, John Wiley & Sons, 2008. DOI:10.1002/9780470512111
- [18] Akin, J.E., Finite element analysis with error estimators, Elsevier, 2005.
- [19] Ahmad, M.; Ismail, K.A., Mat, F., Convergence of Finite Element Model for Crushing of a Conical Thinwalled Tube, Procedia Engineering, (2013) Vol.53, https://doi.org/10.1016/j.proeng.2013.02.075

International Journal of Multiphysics

Volume 18, No. 2, 2024

ISSN: 1750-9548

[20] L.D. Landau, E.M. Lifshitz, and L.P. Pitaevskii, Electrodynamics of Continuous Media, 2nd ed., Elsevier Butterworth-Heinmann, 1984.

- [21] Remski, J.; Zhang, J.; Du, Q., (2014) On balanced moving mesh methods, Journal of computational and applied mathematics, 265, https://doi.org/10.1016/j.cam.2013.09.041
- [22] Huang, W.; Rusell, R.D., Adaptive moving mesh methods, Springer, 2010.